This article has been accepted for publication in IEEE Transactions on Vehicular Technology. This is the author's version which has not been fully edited and content may change prior to final publication. Citation information: DOI 10.1109/TVT.2024.3382729

High-resolution large-scale urban traffic speed estimation with multi-source crowd sensing data

Yingqian Zhang, *Student Member, IEEE*, Chao Li, *Member, IEEE*, Kehan Li, *Student Member, IEEE*, Shibo He, *Senior Member, IEEE*, Jiming Chen, *Fellow, IEEE*

***Abstract*—High-resolution large-scale urban traffic speed estimation is vital for intelligent traffic management and urban planning. However, single-source data from commonly used sources like cameras, loop detectors, or onboard devices exhibit limitations due to uneven distribution and significant noise, especially in large-scale urban areas. Consequently, existing approaches relying on these single-source data often yield low-resolution and biased estimations. In this study, we take the first attempt to leverage mobile pedestrian data and car navigation data for multi-source fusion, proposing a model to achieve high-resolution urban traffic speed estimation in large-scale areas. The key questions are how to obtain and utilize relatively static roadside pedestrian crowd sensing data to characterize the speed of moving vehicles, and how to design multi-source heterogeneous data fusion framework to improve the overall estimation performance. Specifically, a meta-learning-based matrix decomposition algorithm is first proposed to impute the missing values adaptively considering history speed data. After obtaining the imputed data, we utilize the self-view speed aggregation algorithm learning from complete spatial information to correct the imputed values. Subsequently, a multi-view speed aggregation algorithm is proposed to fuse multi-source data for tracking actual road conditions which improves road coverage. We evaluated our model with real-world datasets collected from more than 500,000 smartphones in Wenzhou, China. Experimental results show that the proposed model outperforms the state-of-the-art approaches by 7.48% and 6.99% in MAPE on missing data imputation and multi-source data fusion models, respectively.**

***Index Terms*—Traffic estimation, spatialtemporal data, crowdsensing, data imputation, data fusion**

I. Introduction

HIGH-resolution, large-scale urban traffic speed estimation plays a critical role for the development of intelligent transportation systems. An exhaustive traffic estimation strategy is essential for improving traffic planning and management [1], facilitating rapid detection of traffic incidents [2], and enabling accurate control of traffic signals [3].

Traditional methods of traffic speed estimation, including loop detectors [4], Bluetooth scanners [5], and video cameras [6], have been characterized by their coarse-grained nature, relying primarily on a limited number of dedicated traffic sensing devices strategically placed within confined areas. Evidently, such methods pose significant challenges for fine-grained traffic estimation.

In recent years, mobile phones have become an indispensable tool for navigation [7]. As individuals interact with mapping or ride-hailing applications, their geographical coordinates are captured by providers, yielding an extensive pool of mobile navigation data. The data can be exploited for traffic monitoring and sensing, and has been extensively utilized in traffic state estimation studies [8] [9]. Mobile navigation data is known for its expansive coverage and cost-efficiency. It presents a pronounced divergence from conventional sensing devices, which are generally installed along a restricted number of principal thoroughfares and are associated with significant installation expenses. Regrettably, mobile navigation data fail to provide satisfactory coverage for all road types, presenting higher record densities in hotspots while sparse records in suburban areas [10]. The real-world road network is characterized by a small proportion of hotspots road segments and a majority of less-traveled roads. To compensate this, there is an urgent need for developing advanced traffic speed estimation methodologies that encompass all road types within a city, including suburban and narrow roads, rather than focusing exclusively on main thoroughfares, which facilitates a more comprehensive understanding of the urban traffic conditions.

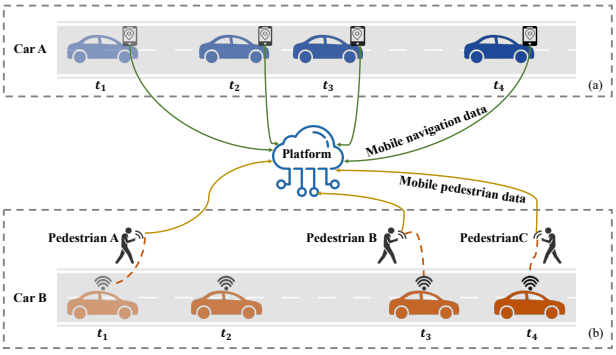

Fig. 1. Multi-source crowdsensing data: (a) Mobile navigation data, (b) Mobile pedestrian data.

In addition to mobile navigation data for navigational purposes, we have noted the widespread adoption of other location-based services by roadside pedestrians [11], including social networking (Weibo, Instagram) and local lifestyle service (Meituan, Yelp) applications, among others. Certain smartphones may receive nearby WiFi signals to enhance localization accuracy while utilizing these services. As a result, the upload information comprises the user's current location and a list of concurrently scanned WiFi networks, some of which originate from nearby vehicle equipment. Fig. 1 depicts the crowdsensing process that randomly accumulates

Yingqian Zhang, Chao Li, Kehan Li, Shibo He, and Jiming Chen are with the Department of Control Science and Engineering, Zhejiang University, Hangzhou, Zhejiang, 310027, China (e-mail: zyq0628@zju.edu.cn; chaoli@zju.edu.cn; khli@zju.edu.cn; s18he@zju.edu.cn; cjm@zju.edu.cn)

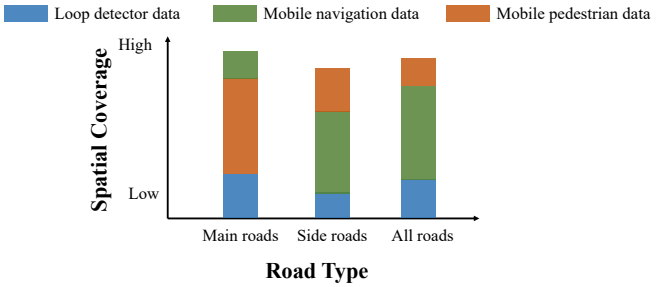

Fig. 2. Comparison of spatial distribution of road sections with different types of data.

a substantial volume of data, termed *mobile pedestrian data*. This data facilitates the estimation of vehicle positions and speeds by sifting through vehicles' WiFi signals using existing databases. Mobile pedestrian data offers a cost-efficient solution without extra sensing devices for broadening the coverage and enhancing the accuracy of urban traffic speed estimations. As demonstrated in Fig.2, a comparison of the spatial distribution of road sections utilizing different data types reveals that mobile pedestrian data exhibit an expanded coverage of pathways, effectively augmenting mobile navigation data. Therefore, the integration of these two data types enhances the coverage and effectiveness for estimation.

This paper is dedicated to the integration of mobile pedestrian and mobile phone navigation data for precise, high-resolution traffic speed estimation. To the best of our knowledge, this work represents the first endeavor to leverage the ubiquitous mobile pedestrian data, gathered through location-based services in smartphone applications, for road state sensing. Nevertheless, integrating these multi-source data to estimate traffic speed presents multiple challenges. First, the sampling location and rate are inherently uncontrollable, resulting in uneven distribution of road data with location and time slots, i.e. data missing in many locations, making it difficult to capture genuine traffic patterns. Second, the integration of multi-source data, inherently accompanied by noise and deviation, poses significant challenges. For instance, mobile phone navigation reports inherently include bias and noise [12]. Similarly, mobile pedestrian data exhibit a clear deviation between roadside pedestrians and passing vehicles, making accurate vehicle position determination more difficult. A straightforward combination of these data sources could potentially amplify estimation inaccuracies.

To address these challenges, we propose an innovative framework combining meta-learning with crowdsensing data fusion for precise, high-resolution traffic speed estimation. Our framework integrates both mobile navigation and pedestrian data. Initially, we use a map-matching algorithm to align each record with corresponding road segment. Next, due to severe initial data missing, we deploy a meta-learning-based matrix decomposition module to impute the imbalanced speed data from various road segments, especially in the considreation of time dimension. This is achieved by calculating a weighted matrix from historical data, where weights are automatically assigned based on the historical data's significance. Consequently, this method obviates the need for reliance on inaccurate fixed prior knowledge [13] or inefficient grid search [14]. After obtaining the imputed data, we utilize the complete spatial information to correct the imputed values. Furthermore, we introduce a speed aggregation module that integrates the multi-view imputed data, deriving the final estimation based on spatial-temporal correlations.

The key contributions of this paper are summarized as follows:

- We have innovatively integrated mobile pedestrian data for traffic speed estimation. By combining mobile pedestrian data, obtained from roadside pedestrians' accidental scanning of vehicle WiFi signals, with mobile phone navigation data, we advance the concept of high-resolution, accurate traffic speed estimation.
- A novel framework is proposed, which includes a meta-learning-based matrix decomposition algorithm and a self-view speed aggregation algorithm to enhance the spatial-temporal coverage. Further, a multi-view speed aggregation module mitigate the impact of data noise and deviation.

The rest of the paper is organized as follows: Section II provides a comprehensive review of related work and Section III introduces the datasets pertinent to our research. In Section IV, we present the methodology and outline our model. Section V discusses the experimental setup and presents the results. Finally, Section VI concludes the paper and highlights avenues for future research.

II. Related Works

A. Traffic Speed Estimation

Traffic speed estimation is important in intelligent transportation system. As more traffic sensing devices are installed, more data have recently become available [15] [16]. Traditionally, traffic estimation mainly rely on various fixed-position road sensors. Loop detectors are primarily employed for collecting traffic count data at fixed positions of a road network. Coifman *et al.* [17] estimation traffic speed estimation from freeway single-loop detectors. However, the loop detectors are sparsely distributed on the road due to high installation and maintenance costs. Traffic sensing devices have been developed in recent years due to their relatively straightforward installation when compared to loop detectors [18]. Yang *et al.* [19] developed a vehicle counting, identification and speed estimation system utilizing RFID backscatter signal. However, there are few vehicles equipped with RFID and the road coverage is still low.

Recently, traffic sensor data such as GPS probe data is widely used. Liu *et al.* [20] realized traffic speed forecasting for segment network with sparse taxi trajectory data. Kan *et al.* [21] examined individual exposures to traffic congestion during various types of trips by using taxi GPS trajectory and POI datasets. Sun *et al.* [22] identified important intrinsic and extrinsic features that impact the bus speed using bus GPS data. Despite the taxi GPS data and bus GPS data have been extensively used, they need specific companies to install equipment for collection.

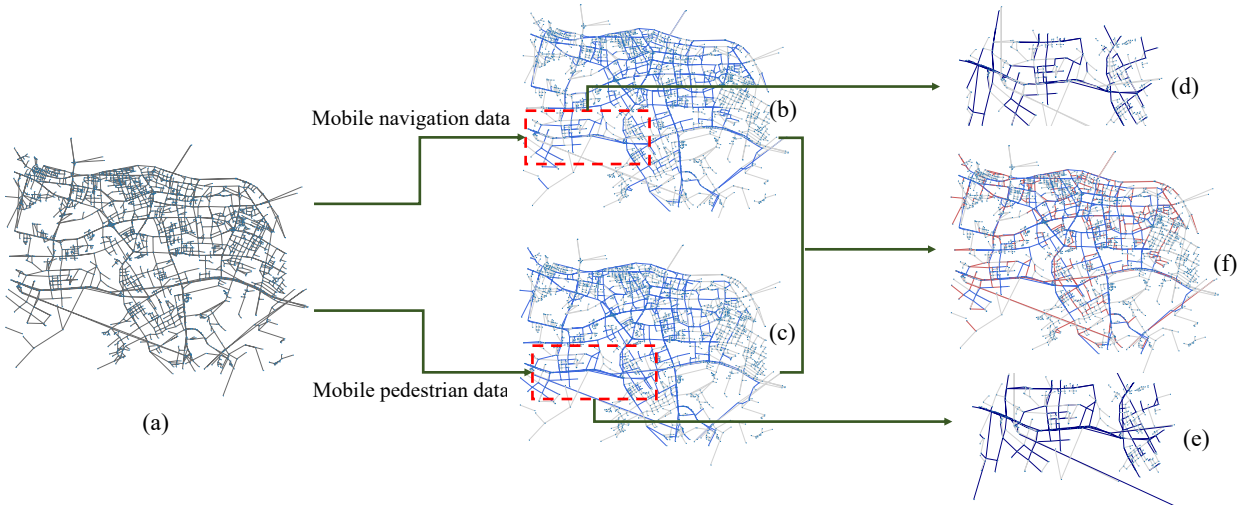

Fig. 3. Daily spatial coverage at 8:00 AM. (a) Initial road network. (b) Covered areas are derived from mobile navigation data, where blue sections represent the roads being passed. (c) Covered areas with mobile pedestrian data where blue sections represent the roads being passed. (d) Amplified areas in the red box in (b). (e) Amplified areas in the red box in (c). (f) Covered areas after data fusion where the red section represents independent sections in a single data source.

Nowadays, mobile GPS data is easy to collect and have been increasingly used [23] [24]. Dong *et al.* [22] presented a traffic speed estimation method based on longest common subsequence. Huang *et al.* [21] proposed a novel human mobility model that combines the advantages of mobile phone signaling data and urban transportation data. Bar-Gera *et al.* [25] examined the performance of a new operational system for measuring traffic speeds and travel times which is based on information from a cellular phone service provider.

B. Data Fusion

The limited representation ability of the single data source restricts its accuracy and coverage in large-scale areas. Some studies have combined multi-source data for traffic state estimation. Generally, data fusion methods can be divided into three categories, statistical methods, probabilistic methods, and neural network methods [26].

Statistical approaches include the weighted average method, correlation analysis, multivariate statistical analysis, and so on. Among them, the arithmetic mean method is the simplest for data fusion. Zhu *et al.* [27] integrated mobile phone network data, inductive loop detector data, and bus-based GPS data by a weighted mean approach in which specific weights such as the inverse of the mean square error (MSE) can be assigned to the various data. Probability methods are usually based on rigorous theories, for example, Kalman filter is mainly used to fuse dynamic multi-source data with noise and Bayesian estimation can produce the probability of a single data source by adopting the mathematical Bayes theorem of probability rule to combine information [28]. Wang *et al.* [1] introduced the Dirichlet process Gaussian mixture model to the generation of the mixed traffic-speed distribution to simultaneously combine taxi GPS data, bus GPS data, and mobile phone GPS data. Lin *et al.* [29] introduced the data fusion method using evidence theory based on the confidence tensor, which reduced the phenomenon of privacy disclosure and ensured the quality of data. The neural network has been proved to be able to extract features and has become popular in various traffic applications. Kuang *et al.* [30] combined the Resnet model with the TCN model to predict traffic volume based on multi-source GPS trajectory data containing the car data coming from the Didi Taxi Platform and the bus data. Peng *et al.* [31] proposed a dynamic graph recurrent convolutional neural network that generates traffic flow forecasting using the historical subway, taxi, and bus data.

Generally, data fusion methods are promising for traffic state estimation problems. However, several critical questions, e.g., the effective fusion of data with noise, the complete extraction of correlations within datasets, which remain unsolved.

III. Preliminary

A. Geographic Information Data

The geographic information data of the road network utilized in this study is collected from the central districts of Wenzhou, Zhejiang Province, China. The data is sourced from OpenStreetMap (OSM) [1]. The road network comprises 62851 road segments and 25449 intersections in which the name, type, and length of each road are recorded.

B. Crowdsensing Data

The anonymous implicit crowdsensing data used in this article is provided by Westlake Institute for Data Intelligence [2], which is collected by crowdsensing platforms of location-based services providers embedding on location-based service from March 21, 2020, to March 28, 2020. The data collection is authorized by anonymization smartphone users and unconstrained without infringing users' privacy and smartphone battery. Note that the frequency of uploading varies significantly

[1] www.openstreetmap.org
[2] https://www.widi.org.cn/

TABLE I. Crowdsensing dataset.

Variable name	Description
Gid	User's id
Timestamp	User reporting time
Lon	User's longitude
Lat	User's latitude
App list	List of Apps
WiFi list	List of scanned WiFi

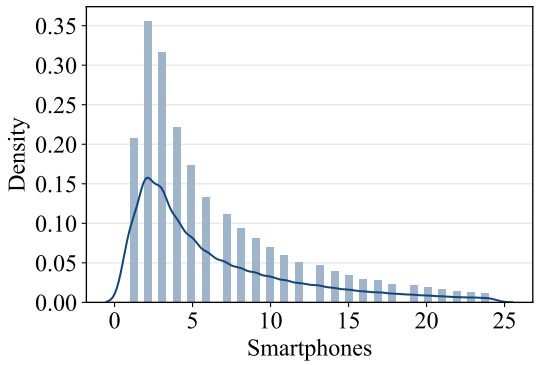

Fig. 4. The distribution of the number of smartphones scanning vehicle in mobile pedestrian data.

among smartphone users, spanning from seconds to minutes. Each record of data r_i contains six properties: user-id $r_{i,u}$, longitude $r_{i,\lambda}$, latitude $r_{i,\varphi}$, timestamp $r_{i,t}$, APP usage list r_{i,l_A} and scanned WiFi list r_{i,l_W}, which are listed in Table I.

The mobile navigation data is sourced from commonly used navigation application such as Amap[3] and DiDi[4], installed on smartphones. To procure this data, we filtered the application usage lists in the raw data.

On the other hand, the mobile pedestrian data is gathered when roadside pedestrians incidentally scanned vehicle WiFi signals with their smartphones. This data collection process involves filtering the scanned WiFi lists in the raw data. Notably, roadside pedestrians can be considered as quasi-static sensors along the road, given their relatively slow movement.

The distribution reflecting the frequency of smartphones scanning vehicles in the mobile pedestrian dataset is depicted in Fig. 4. Ordinarily, the WiFi signal of a vehicle during transit is detected by approximately five smartphones belonging to roadside pedestrians. As a result, by harnessing the records from these pedestrians, we can effectively estimate the trajectory information of the vehicles.

It should be noted that the distribution of records in both mobile navigation and pedestrian data varies daily, as illustrated in Fig. 5(a). Specifically, navigation data exhibit a higher number of records during off-peak times, while there are more pedestrian data during rush hours but very little data during off-peak times. Besides, as illustrated in Fig. 5(b), the temporal pattern of the two types of data also exhibits notable differences. The time skip distribution of mobile navigation entries is predominantly concentrated around specific values, whereas the pedestrian dataset exhibits a more homogeneous distribution. These differences underscore the intrinsic characteristics and distinctiveness of each data type.

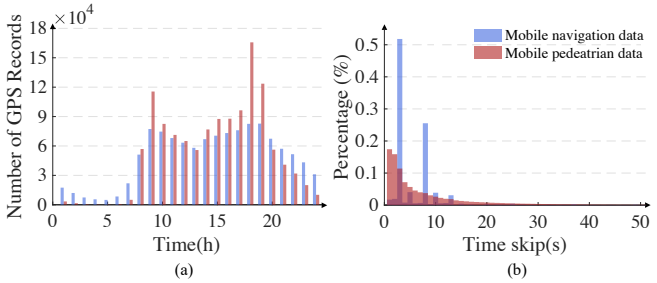

Fig. 5. (a) GPS records' volume for mobile navigation data and mobile pedestrian data. (b) Distributions of time intervals between two consecutive records.

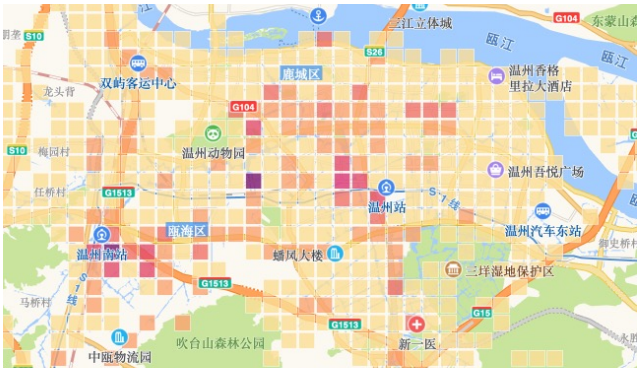

(a)

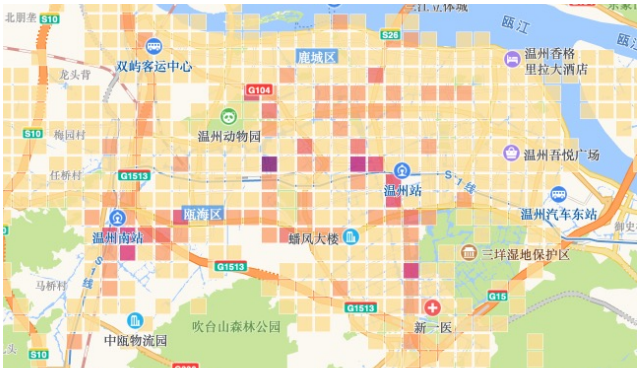

(b)

Fig. 6. Thermal distribution of roads. (a) Mobile navigation data, (b) Mobile pedestrian data.

C. Preprocessing

We have processed the original crowdsensing data and apply a spatial map-matching algorithm [32] to map the trajectories to the road network, resulting in the generation of the original estimated navigation speed data and pedestrian speed data. To evaluate the road coverage afforded by different datasets during the period from 8:00 AM to 8:30 AM, we calculated the coverage statistics, which are delineated in

[3]https://www.amap.com/
[4]https://www.didiglobal.com/

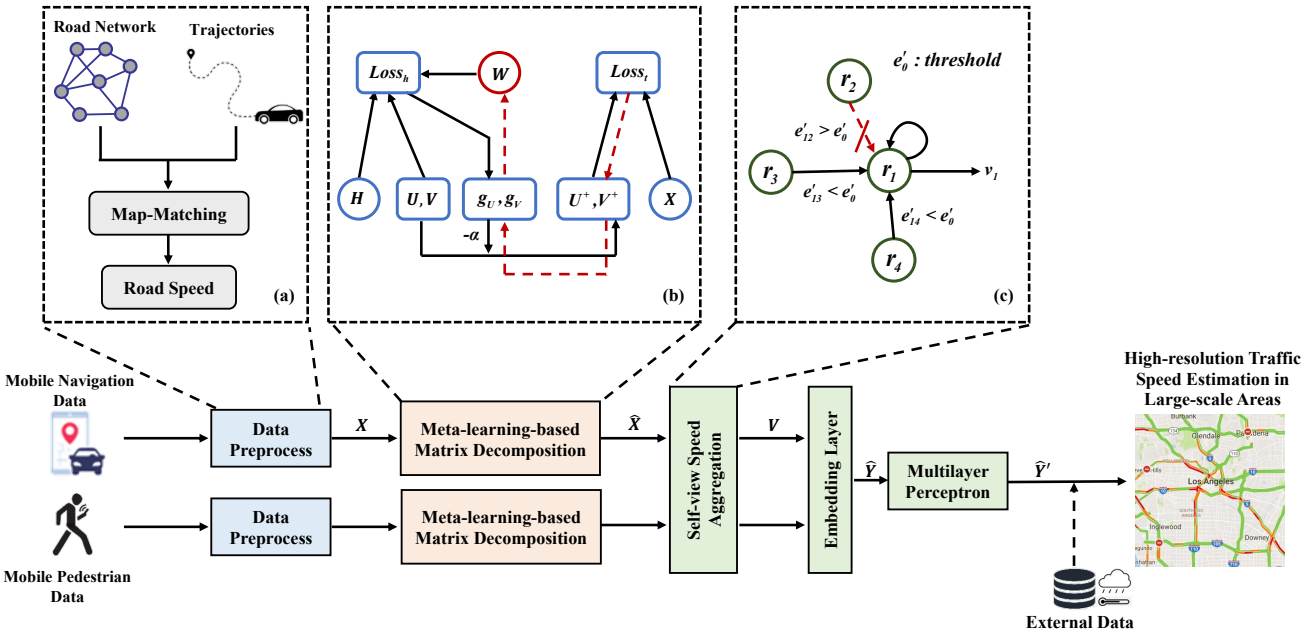

Fig. 7. System framework. (a) is the structure of data preprocessing. (b) is the detailed structure of meta-learning-based matrix decomposition. The meta-learning process of the weighing matrix composes of two forward-backward passes. It firstly uses history speed matrix **H** to compute the weighted loss. Then gradient on **U**, **V** is computed from $Loss_h$ to update the matrix decomposition function for one gradient step. The speed target matrix X and the updated matrix decomposition function are used to compute $Loss_t$. At last, we update **W** by gradient-on-gradient on $Loss_t$. (c) is the example of self-view speed aggregation which adaptively aggregates neighboring information.

Table II. Our analysis reveals that data from different sources are dominant in different road sections, respectively, rather than consistently outperforming each other in all situations. In particular, the navigation data predominantly concentrates on major thoroughfares, whereas the pedestrian data is more uniformly dispersed, as evidenced in Fig. 3. Notably, Fig. 3 (a) represents the initial road network, Fig. 3 (b) and Fig. 3 (c) depict the covered areas derived from navigation data and pedestrian data, respectively, where blue sections represent the roads being passed. Further, Fig. 3 (d) and Fig. 3 (e) showcase the amplified areas. These visualizations suggest that data procured from varied sources possess the potential to mutually enhance spatial and temporal coverage, as shown in Fig. 3 (f), where the red section represents independent sections in a single data source. We observe the existence of uncovered areas in both navigation and pedestrian data. Consequently, it is imperative to first impute the missing data of each source and subsequently integrate the multi-source imputed data.

Additionally, we have created thermal distribution plots for both the navigation and pedestrian datasets, as illustrated in Fig. 6. The intensity of the color corresponds to the level of heat density in the area. It is observable that the thermal variance is more pronounced across different regions in the navigation dataset, whereas the pedestrian dataset demonstrates a more consistent and homogenous distribution. The efficient fusion of these two types of data holds the potential to yield improved estimation results.

IV. Methodology

The proposed traffic speed estimation framework is illustrated in Fig. 7. Firstly, a meta-learning-based matrix decomposition is designed to impute the missing speed data mostly in consideration of temporal correlation, due to severe initial data missing,. Upon acquiring the comprehensive set of imputed data, we introduce a self-view speed aggregation module designed to employ spatial information for the correction of imputed values. Finally, we fuse the multi-view imputed data to effectively generate the final estimated speed in a large-scale road network. The detailed methodology is introduced in the following.

TABLE II. Coverage performance comparison for different datasets from 8:00 AM to 8:30 AM.

Data type	Mobile navigation	Mobile pedestrian	Taxi
All roads	80.14%	81.52%	83.12%
Primary	92.26%	91.44%	96.25%
Secondary	87.65%	88.24%	93.24%
Tertiary	79.76%	83.49%	80.12%
Others	70.00%	70.79%	77.89%

A. Meta-Learning-based Matrix Decomposition

Meta-learning algorithms have primarily been developed for few-shot learning, focusing on data efficiency by facilitating information transfer across related tasks [33] [34] and the context of learning to optimize [35] [36]. Gradient-based meta-learning and hyperparameter optimization [37] has been proved effective to solve a bilevel optimization problem. In this paper, we aim to find the proper weights of history data during matrix decomposition instead of manually setting fixed parameters or through grid-search which is time-consuming

and difficult to find the optimal value. The methodology of employing historical data to address the issue of missing data via updates to the weight matrix and matrix decomposition is in harmony with the principles of gradient-based meta-learning. Consequently, we take advantage of the meta-learning algorithm to learn from historical data and automatically assign weights to different training examples according to their significance, as shown in Fig. 7(b). The meta-learning process for the weighted matrix utilizes a gradient-on-gradient approach, which propagates gradients from a target loss incurred in current matrix decomposition to the weighted matrix, thereby learning from historical data.

We infer the missing traffic speed data on particular road segments at specific time intervals by a target speed matrix $\mathbf{X} \in R^{m \times n}$. The spatial dimension indicates specific spatial road segments, where m is the number of road segments that have been recorded. The temporal dimension indicates the specific time intervals (e.g., a 5-min time interval from 0:00 AM to 0:05 AM), where n is the number of continuous observation time intervals. Each entry in $\mathbf{X}$ indicates the mean speed in a spatial road segment m during a time interval n of the day. We introduce mask matrix $\mathbf{M} \in R^{m \times n}$ to indicate the missing entries of $\mathbf{X}$:

$$\mathbf{M}_{i,j} = \begin{cases} 1, & if \ \ \mathbf{X}_{i,j} \ \ is \ \ available \\ 0, & if \ \ \mathbf{X}_{i,j} \ \ is \ \ missing. \end{cases} \tag{1}$$

A common approach to impute the missing data is decomposing the matrix into two matrices. For example, we can decompose $\mathbf{X}$ into the multiplication of $\mathbf{U} \in R^{m \times q}$ and $\mathbf{V} \in R^{n \times q}$ and recover the complete speed matrix $\widehat{\mathbf{X}} \in R^{m \times n}$ by introducing $\mathbf{U}\mathbf{V}^T$:

$$\min_{\mathbf{U},\mathbf{V}} \frac{1}{2} \left\| \mathbf{M} \odot (\mathbf{X} - \mathbf{U}\mathbf{V}^T) \right\|^2 + \lambda \left\| \mathbf{U} \right\|^2 + \lambda \left\| \mathbf{V} \right\|^2 \tag{2}$$

$$\widehat{\mathbf{X}} = \mathbf{M} \odot \mathbf{X} + (1 - \mathbf{M}) \odot \mathbf{U}\mathbf{V}^T \tag{3}$$

where $\odot$ denotes element-wise multiplication, $\|\cdot\|^2$ denotes the L_2 norm, $\lambda \left\| \mathbf{U} \right\|^2 + \lambda \left\| \mathbf{V} \right\|^2$ is a regularization of penalties to avoid over-fitting, q denotes the number of latent factors which is smaller than m,n , and λ is a parameter controlling the contributions of the regularization. However, in our situation, the matrix is over sparse at a large scale. For example, if we set 5 minutes as a time interval, only 25.5% and 23.2% entries of $\mathbf{X}$ are available on navigation and pedestrian speed data separately, which leads to unsatisfied performance.

As a result, we use historical data over a long period (e.g., one week) to establish the history speed matrix $\mathbf{H} \in R^{m \times n}$, which provides additional information for our decomposition, i.e., traffic patterns in the road network. An entry in $\mathbf{H}$ indicates the mean speed in a spatial road segment m during a time interval n in historical records. We introduce another mask matrix $\mathbf{N} \in R^{m \times n}$ to indicate the missing entries of $\mathbf{H}$:

$$\mathbf{N}_{i,j} = \begin{cases} 1, & if \ \ \mathbf{H}_{i,j} \ \ is \ \ available \\ 0, & if \ \ \mathbf{H}_{i,j} \ \ is \ \ missing. \end{cases} \tag{4}$$

We define a weighting matrix $\mathbf{W} \in R^{m \times n}$ to measure the importance of each entry in $\mathbf{H}$. Then, we obtain the complete speed matrix $\widehat{\mathbf{X}}$ by decomposing $\mathbf{X}$ with $\mathbf{H}$, $\mathbf{W}$, $\mathbf{M}$, and $\mathbf{N}$. Specifically, $\widehat{\mathbf{X}}$ will be trained with the unweighted loss on target speed matrix $\mathbf{X}$ and weighted loss on history speed matrix $\mathbf{H}$, $\mathbf{W}$ will be trained by meta-learning using gradient-on-gradient.

We first decompose $\mathbf{X}$ into $\mathbf{U}$ and $\mathbf{V}$, as mentioned in Equ.(2) to obtain an initialization for the following training. We aim to give more weight to history speed data with similar speed patterns of the day. Thus we set the weighted loss function as:

$$\begin{aligned} Loss_h(\mathbf{W}) = \frac{1}{2} \left\| \mathbf{W} \odot \mathbf{N} \odot \left(\mathbf{H} - \mathbf{U}\mathbf{V}^T \right) \right\|^2 \\ + \lambda \|\mathbf{U}\|^2 + \lambda \|\mathbf{V}\|^2 \end{aligned} \tag{5}$$

The loss on history speed data can be regarded as a function of $\mathbf{W}$, and we take the derivative of $Loss_h$($\mathbf{W}$ with respect to $\mathbf{U}$ and $\mathbf{V}$):

$$g_{\mathbf{U}}(\mathbf{W}) = \frac{\partial Loss^h(\mathbf{W})}{\partial \mathbf{U}} \tag{6}$$

$$g_{\mathbf{V}}(\mathbf{W}) = \frac{\partial Loss^h(\mathbf{W})}{\partial \mathbf{V}} \tag{7}$$

$\mathbf{U}$, $\mathbf{V}$ is then updated by one gradient descent with learning rate α:

$$\mathbf{U}^+(\mathbf{W}) = \mathbf{U} - \alpha g_{\mathbf{U}}(\mathbf{W}) \tag{8}$$

$$\mathbf{V}^+(\mathbf{W}) = \mathbf{U} - \alpha g_{\mathbf{V}}(\mathbf{W}) \tag{9}$$

Meta-learning algorithm is closely related to the learn-to-learn idea, which updates the parameters in the former task for the further new tasks. We argue that the learning of the weighting matrix should only minimize the loss on the target speed data to reduce the decomposition loss in the last step. As a result, we construct a loss by a forward pass on matrix decomposition with the target speed data based on $\mathbf{U}^+$ and $\mathbf{V}^+$:

$$\begin{aligned} Loss_t(\mathbf{W}) = \frac{1}{2} \left\| \mathbf{M} \odot (\mathbf{X} - \mathbf{U}^+ (\mathbf{V}^+)^T) \right\|^2 \\ + \lambda \left\| \mathbf{U}^+ \right\|^2 + \lambda \left\| \mathbf{V}^+ \right\|^2 \end{aligned} \tag{10}$$

Then, we compute the derivative of $Loss_t(\mathbf{W})$ with respect to $\mathbf{W}$ by gradient-on-gradient and update $\mathbf{W}$ with learning rate β:

$$\begin{aligned} g_{\mathbf{W}} = \frac{\partial \operatorname{Loss}^t(\mathbf{W})}{\partial \mathbf{W}} = \frac{\partial \operatorname{Loss}^t(\mathbf{W})}{\partial \mathbf{U}^+(\mathbf{W})} \frac{\partial \mathbf{U}^+(\mathbf{W})}{\partial \mathbf{W}} \\ + \frac{\partial \operatorname{Loss}^t(\mathbf{W})}{\partial \mathbf{V}^+(\mathbf{W})} \frac{\partial \mathbf{V}^+(\mathbf{W})}{\partial \mathbf{W}} \end{aligned} \tag{11}$$

$$\mathbf{W}^+ = \mathbf{W} - \beta g_{\mathbf{W}} \tag{12}$$

After iteratively updating, we access a well-learned weighting matrix $\mathbf{W}$, we can impute the missing data using both the target speed data $\mathbf{X}$ and the history speed data $\mathbf{H}$. We adopt the function for training the matrix decomposition module as:

$$\begin{aligned} \min_{\mathbf{U},\mathbf{V}} \frac{1}{2} \left\| \mathbf{M} \odot (\mathbf{X} - \mathbf{U}\mathbf{V}^T) \right\|^2 + \frac{1}{2} \left\| \mathbf{W} \odot \mathbf{N} \odot \left(\mathbf{H} - \mathbf{U}\mathbf{V}^T \right) \right\|^2 \\ + \lambda \left\| \mathbf{U} \right\|^2 + \lambda \left\| \mathbf{V} \right\|^2 \end{aligned} \tag{13}$$

Finally, we approximate the desired complete matrix as mentioned in Equ.(3).

B. Speed Aggregation with Imputed Data

Although we have obtained the imputed data from the previous section, the quality of imputed data is uncertain, and simply fusing the multi-source data might lead to an undesirable result. Therefore, this section proposed a self-view speed aggregate module and multi-view speed aggregate module to output the estimated speed effectively.

1) Self-View Speed Aggregation: We are unable to ascertain spatial correlations from sparse data until fully imputed datasets are obtained. Once the imputation is complete, it becomes feasible to evaluate whether the velocity of the central road segment aligns with the speed fluctuations of its adjacent roads. In this section, we use self-view speed aggregation to further improve the quality of data estimation based on the spatial relationship between adjacent road segments.

Spatial dependencies exist between road segments in the road network, where the states of roads are influenced by the surrounding. For example, if a traffic accident occurs in the surrounding road segments, the flow of the center road segment would possibly increase, resulting in slower traffic speed. We calculate the euclidean distance between any two roads' speed lists and the geographical distance between corresponding road segments. Fig. 8 shows the correlation between the road spatial distance and the road speed difference. The closer the geographical distance of the road segments, the greater the speed similarity; in the meantime, the farther the distance, the greater the difference. As a result, we adopt a self-view speed aggregation module to capture the spatial correlation between neighboring roads. It aggregates the central road speed with its adjacent road speed, which correlates highly to the central road.

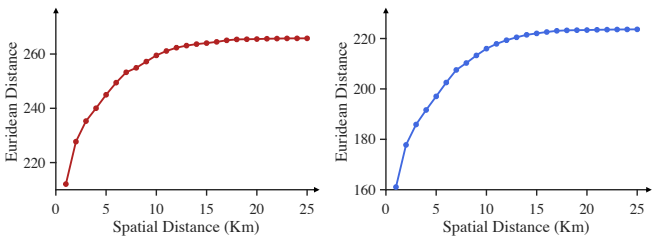

Fig. 8. Spatial speed correlation of road segments in the network: (a) Mobile navigation data, (b) Mobile pedestrian data.

Instead of setting the fixed coefficient of neighboring roads and equally aggregating neighboring roads' speed, we innovatively improve the effectiveness by dynamically adjusting the dependencies between roads. We use history speed data to quantify the spatial dependencies between roads. Firstly, we impute the missing data in $\mathbf{H}$ to obtain the complete history speed data $\widehat{\mathbf{H}} \in R^{m \times n}$ by matrix decomposition similar to Equ.(2) and Equ.(3). To extract the diverse spatial correlation, the spatial dependencies e'_{ij} between the road segment r_i and road segment r_j can be formulated as:

$$e'_{ij} = \sqrt{\sum (\widehat{H}_{i,:} - \widehat{H}_{j,:})^2} \quad j \in N_i \tag{14}$$

where N_i is the set of neighboring connected roads for the r_i that shares the common intersection with it.

If the historical speed trend of adjacent connecting roads differs significantly from the historical speed of the central road, we consider that the correlation between these two roads is small. Thus the central road does not require any information from unnecessary adjacent connecting roads. It would retain its existing information rather than permanently fuse neighboring information:

$$e_{ij} = \begin{cases} +\infty, & e'_{ij} > \text{ threshold} \\ e'_{ij}, & e'_{ij} \leq \text{ threshold} \end{cases} \tag{15}$$

where e_{ij} indicates the adjusted spatial speed dependence between the r_i and r_j. The threshold is defined as the upper quartile in e'.

We perform consistency processing on the adjusted spatial speed dependence, and then reassign the dependence weights of each road segment. The magnitude of the dependence between a specific center road section and its surrounding bordering road sections may be significant. However, we assign weights based on the relative magnitude of the values rather than their absolute magnitude. This approach prevents inaccuracies that may arise from changes in the numerical scale. We have the explicit formulation of the weighted fusion coefficient a_{ij} computed as:

$$a_{ij} = \frac{\exp\left(-e_{ij}/k\right)}{\sum_{j=N_i} \exp\left(-e_{ij}/k\right) + \varepsilon} \tag{16}$$

where k represents a scalar, and we introduce $\varepsilon = 10^{-7}$ to avoid overflow. We obtain the weighted fusion coefficient through measuring the proportion of dependency between each road segment and the central road segment to all adjacent road segments. The higher the proportion, the closer the relationship between the two road sections in reality.

The aggregation step outputs the self aggregated speed $\mathbf{V} \in R^{m \times n}$, which sticks to useful neighbor information and keeps information itself at the same time instead of absolutely depending on surrounding:

$$\mathbf{V}_{i,:} = (1 - \sum_{j=N_i} \frac{a_{ij}}{2}) * \widehat{\mathbf{X}}_{i,:} + \sum_{j=N_i} \frac{a_{ij}}{2} * \widehat{\mathbf{X}}_{j,:} \tag{17}$$

2) Multi-View Speed Aggregation: Multi-view speed aggregation module aims to fuse multi-view imputed speed data and output the final results. We have already received the adjusted navigation speed data $\mathbf{V}_d \in R^{m_d \times n}$ and pedestrian speed data $\mathbf{V}_w \in R^{m_w \times n}$, where m_d is the number of road segments traveled in navigation data and m_w is in pedestrian data. We intend to simultaneously combine adjusted navigation speed data and pedestrian speed data to get the final estimated traffic speed $\widehat{\mathbf{V}} \in R^{m_a \times n}$, which improves the spatial coverage and the accuracy of traffic speed estimation, where m_a is the number of road segments traveled in navigation data or pedestrian data that $m_a = m_d \cup m_w$.

Firstly, we expand the two-dimensional speed matrix $\mathbf{V}_d$ and $\mathbf{V}_w$ into one-dimensional vector $\mathbf{v}_d \in R^{(m_d \times n) \times 1}$ and $\mathbf{v}_w \in R^{(m_w \times n) \times 1}$. Except for the feature of speed value, we denote $\mathbf{F}_d \in R^{(m_d \times n) \times 2}$, $\mathbf{F}_w \in R^{(m_w \times n) \times 2}$ as additional feature matrices, where 2 is the number of additional features. We select the timestamp and whether the speed is imputed as additional features since the speed change is closely related

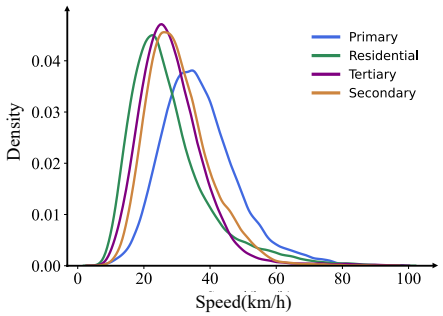

Fig. 9. Speed distribution of different road types.

to the current timestamp that the overall speed during peak hours is slower. In addition, the performance of the two data modalities fluctuates across various time intervals. For instance, the volume of mobile pedestrian data in the early morning is comparatively limited, which consequently affects the relative quality of estimation. Accordingly, during the fusion process, the weighting assigned to such data diminishes during these periods. Further, we default that the imputed data has lower reliability than the data directly obtained from sensors, thus, the relative proportion in the fusion will be lower. In reality, over 70% of the dataset is missing. As a result, although the experimental protocol may assign a greater weight to authentic data, it will not cause the imputed data to lose its effectiveness. To facilitate the follow-up training, we extend the horizontal axis dimension of vectors and matrices by $m_a \times n$, where the extra filling values are 0.

Since the additional feature is discrete variable, the implementation needs to convert it into a set of one hot vectors. Then we introduce an embedding layer for mapping concatenated additional features to continuous number vector features:

$$\mathbf{H} = Onehot(Concat(\mathbf{F}_d, \mathbf{F}_w)) \tag{18}$$

$$\mathbf{Z} = \mathbf{W}\mathbf{H} \tag{19}$$

$\mathbf{W}$ is the weighting matrix and $\mathbf{Z} \in R^{(m_a \times n) \times e}$, where e is the number of projected latent features in the embedding layer.

Finally, the embedding features are concatenated with continuous speed features, which are later fed into a Multilayer Perceptron (MLP) that consists of three linear transformations adopting 3,2,1 neurons for each with a ReLU activation in between:

$$\widehat{\mathbf{Y}} = MLP(Concat(\mathbf{Z}, \mathbf{v}_d, \mathbf{v}_w)) \tag{20}$$

where $\widehat{\mathbf{Y}} \in R^{(m_a \times n) \times 1}$ is the fusion speed.

At last, we correct the estimated speed by the external factor (i.e., road type). According to historical data, we can easily obtain the velocity distribution of each type of road shown in Fig. 9. We regard the velocity distribution as a normal distribution approximately with the expectation μ and variance σ of each type of road. It is almost impossible that the particular speed is outside the range $(\mu \pm 1.960\sigma, 95\%)$ [38] [39]. As a result, if the speed of a specific road segment is out of range, we correct the speed to be consistent with the distribution and output the final desired estimated traffic speed $\widehat{\mathbf{Y}}' \in R^{(m_a \times n) \times 1}$.

V. Experiment Result

In this section, we conduct a comprehensive performance evaluation to thoroughly validate the proposed speed estimation model using real-world datasets. Furthermore, we compare the performance of our model with that of state-of-the-art methods to establish its effectiveness and superiority.

In the experiment, we divide a single day into 288 time-episodes (with a time interval of 5 minutes). We observe that data coverage fluctuates considerably at various times throughout the day. Notably, the navigation data maintains stability around the busiest periods, whereas the pedestrian data demonstrates extensive coverage during peak hours but undergoes a marked decline post-peak. Fig. 10(a)-(b) depict the coverage variance of tertiary roads by the two data modalities during morning and evening rush hours. In Fig. 10(c)-(d), pie charts are employed to depict the coverage number of road segments within the dataset, with the intersecting central section denoting the quantity of road segments that are jointly encompassed by both data types. The graph indicates that during the morning peak hours, the navigation data encompasses a greater number of roads, whereas the coverage is more extensive in the pedestrian data at noon. Consequently, navigation and pedestrian data exhibit mutual complementary at distinct temporal junctures.

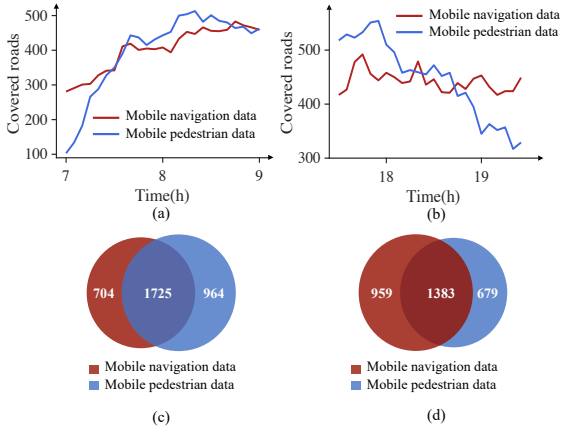

Fig. 10. (a)-(b) Data coverage difference at tertiary roads. (c) Data coverage difference at 8:00 AM. (d) Data coverage difference at 12:00 PM.

A. Measures of Effectiveness

We employ the taxi data encompass trajectories of more than 3000 taxies in the city of Wenzhou during the same period from March 21, 2020, to March 28, 2020, as the ground truth, which is a practice common to the majority of extant methods. The real-time location of each taxi is collected and recorded at 20-second intervals, generating over 10 million GPS records each day. Taxi data encompasses a substantial portion of road segments, and we will compare the results with the road segments with taxi data.

In this paper, we employ three measures of effectiveness to conduct a quantitatively evaluation of the performance of our

TABLE III. Performance comparison for different data imputation methods.

Results comparison on different data						
Models	Mobile navigation data			Mobile pedestrian data		
	MAE	RMSE	MAPE	MAE	RMSE	MAPE
Unprocessed	8.538	11.242	28.134	9.223	12.043	30.990
Interpolate	8.830	11.745	29.016	9.470	12.396	31.430
KNNImputer	8.543	11.312	27.757	9.282	12.138	30.698
GAIN	8.941	12.078	29.108	10.315	13.875	33.094
LRTC	8.590	11.235	30.261	9.150	11.881	32.616
GAIN	8.941	12.078	29.108	10.315	13.875	33.094
SAITS	10.336	13.997	33.403	10.217	13.941	32.648
LRMC-ILM	8.463	11.255	27.509	9.072	11.920	29.924
Proposed method	**8.186**	**10.828**	**26.690**	**8.812**	**11.521**	**29.014**

TABLE IV. Performance comparison for different data fusion methods.

Models	MAE	RMSE	MAPE
WMA	7.896	10.459	25.706
IMVC	7.635	10.197	25.340
LR	7.467	10.094	25.901
GBDT	7.345	**9.740**	25.779
Proposed method	**7.320**	9.837	**23.877**

proposed algorithm against other benchmark methods. We test the model with Mean absolute percentage error (MAPE) as:

$$\mathrm{MAPE} = \frac{100\%}{n}\sum_{i=1}^{n}\frac{|\hat{y}_i - y_i|}{y_i} \tag{21}$$

where $\hat{y}_i$ is the estimated speed value, y_i is the verified real speed value provided by taxi GPS data as ground truth and n is the number of all estimated values.

To further evaluate the performance of the model, we also provide Mean absolute error (MAE) and Root Mean Squared Error (RMSE) as compared:

$$\mathrm{MAE} = \frac{\sum_{i=1}^{n}|\hat{y}_i - y_i|}{n}, \tag{22}$$

$$\mathrm{RMSE} = \sqrt{\frac{\sum_{i=1}^{n}(\hat{y}_i - y_i)^2}{n}}. \tag{23}$$

Specifically, MAPE utilizes percentages to measure the deviation, making it less susceptible to the influence of extreme values, and it does not need to be combined with the dimension of real value to judge the difference.

B. Missing Data Imputation

The data imputation algorithm described in Section IV is employed to impute the missing speed data for road segments that have records on March 28, 2020. To augment the model with additional speed pattern insights, historical data from both navigation and pedestrian sources covering March 21, 2020, to March 27, 2020, are utilized. The observed spatial-temporal

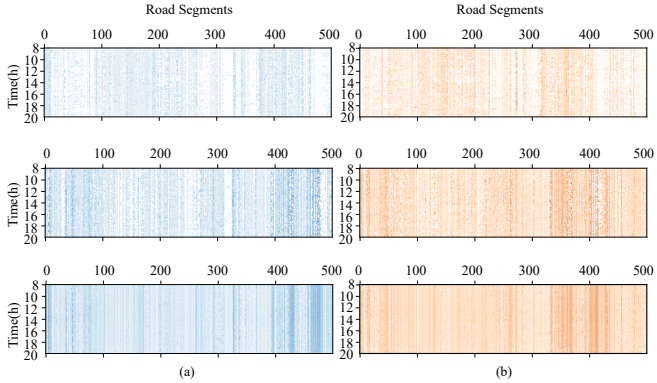

Fig. 11. Visualization of spatial-temporal missing data imputation effect: (a) From top to bottom are mobile navigation data with missing value, historical mobile navigation data and imputed mobile navigation data. (b) From top to bottom are mobile pedestrian data with missing value, historical mobile pedestrian data and imputed mobile data.

missing rates in the navigation and pedestrian datasets are 74.5% and 76.8%, respectively, over the entire day. Remarkably, after data imputation, the spatial-temporal coverage rates in the navigation and pedestrian datasets surged from 25.5%, 23.2% to 100%, 100% each. This suggests that through the data imputation algorithm, we can estimate the speed of road segments as long as they are recorded in the historical data(i.e., large-scale urban traffic speed estimation), thereby enhancing coverage.

To be specific, we set the learning rate α to $1e-4$ and the value of β to $1e-4$. The Adam optimizer is utilized with

$\beta_1 = 0.9$ and $\beta_2 = 0.999$. Initially, we pretrain the normal matrix decomposition for 10K steps to ensure a favorable initialization. Subsequently the meta-learning process for the weighting matrix is executed for 30,000 epochs. Finally, we train the meta-learning-based matrix decomposition for 10K steps. The performance is compared with five other state-of-the-art imputation methods:

- SAITS [40] is based on the self-attention mechanism for missing value imputation in multivariate time series.
- LRMC-ILM [20], the Improved Low-rank Minimization problem in matrix completion, attends to impute the missing speed data with consideration to nonlinear spatial and temporal correlations.
- LRTC [41], low-rank tensor completion, improves single-source data by constructing a 3D tensor and performing context-aware decomposition.
- GAIN [42] adapts the well-known GAN model to minimize the difference between the original and imputed data.
- Interpolation imputation [43] based on data distribution.
- KNN Imputation [44] selects k nearest neighbors for each missing data via calculating the gray distance between the missing datum to iteratively imputes missing data.

Our proposed approach demonstrates marked superiority relative to each benchmark method across all metrics within both the navigation and pedestrian datasets. Significantly, we note an enhancement in performance during morning and evening peak periods, attributed largely to the profusion of record data available. Conversely, during the early hours and late night, the efficacy of the approach is somewhat diminished, attributable to the paucity of data during these intervals.

Further, we visualize the efficacy of our proposed model in imputing missing spatial-temporal data. Fig. 11 presents, from top to bottom, datasets with missing values, historical data, and imputed data, in that order. The figure delineates 500 randomly selected road segments on the x-axis and 12h time steps, corresponding from 8AM to 8PM period, on the y-axis. Among them, historical data represents the average speed of a certain road segment at a certain time based on all records in the past. There are situations where road segments have no records in some time periods. In this depiction, voids represent missing data while the intensity of the color indicates the speed values. Fig. 11 reveals that the imputed data effectively draws inspiration from historical data data but not limited to historical data. Despite the richness of information in historical datasets, they still can do not provide complete coverage. Our data imputation method improves the dataset based on historical data and actual situations. The imputed data aligns well with the actual road conditions, i.e., segments with historically higher speeds also exhibit correspondingly elevated imputed speeds. Nevertheless, our proposed model effectively capture the speed pattern knowledge even under sever data scarcity conditions, enabling accurate speed data imputation for any road at any time, related to high-resolution estimation goal.

C. Multi-Source Data Fusion

In this section, we utilize a speed aggregation algorithm to estimate the traffic speed using the recovered data. The timeframe for the current study period and the historical information period employed herein aligns with the interval utilized for data imputation in the previous sections

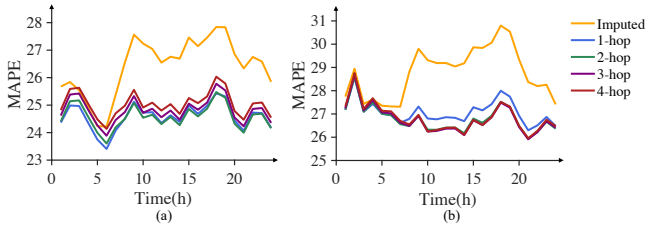

Fig. 12. Comparison of estimation performance under various hops in MAPE: (a) Mobile navigation data, (b) Mobile pedestrian data.

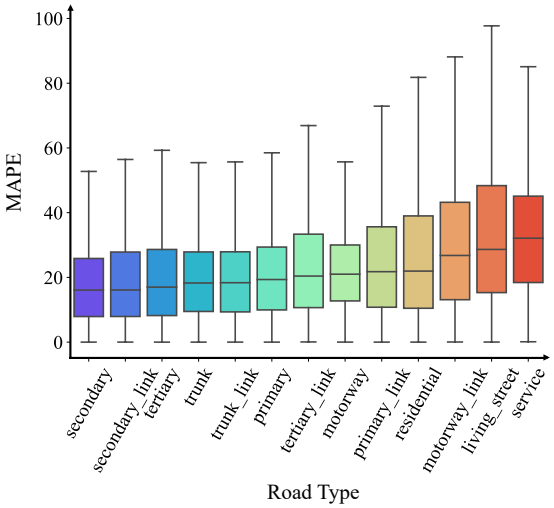

Fig. 13. Comparison of estimation performance under various types of roads in MAPE.

Fig. 12 illustrates the enhanced performance achieved through the utilization of the self-view speed aggregation module. The proposed self-view speed aggregation module demonstrates a remarkable improvement in accuracy, with a minimum increase of 8.29% and 8.02% in MAPE for both navigation data and pedestrian data. The improvement is particularly evident during periods of abundant data. It is obvious that road segments within a one-hop range exhibit a high degree of inter-connectivity with the central road section. Thus, leveraging the neighboring segments' information can significantly improve the estimation of the central road segment.

Furthermore, we conducted a comparison of the aggregation effect with different hops of neighboring information. Interestingly, we observed that with the increase of integrated information, the aggregation effect may either decline or exhibit only marginal improvements. Hence, in this study, we aggregate one-hop neighbors' information, which adequately captures the correlation between road segments.

To demonstrate the performance of the multi-view Speed aggregation module, we randomly partitioned the data from

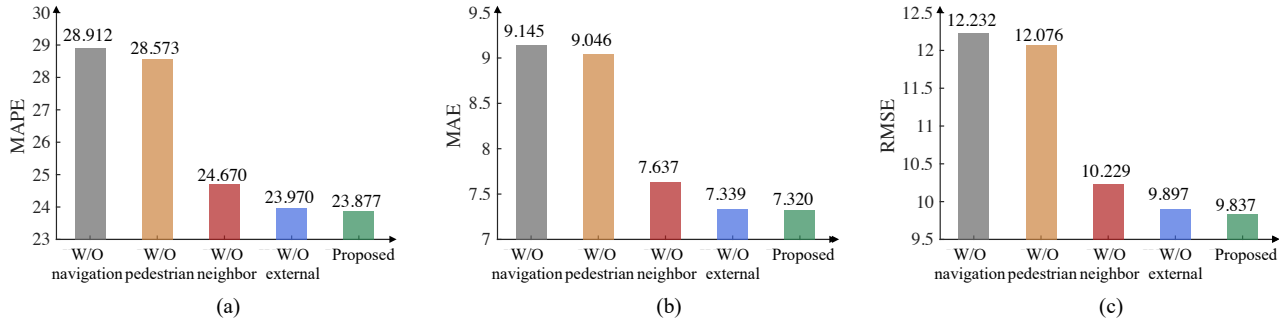

Fig. 14. Performance comparisons over the proposed model and its variants: (a) in MAPE, (b) in MAE and (c) in RMSE.

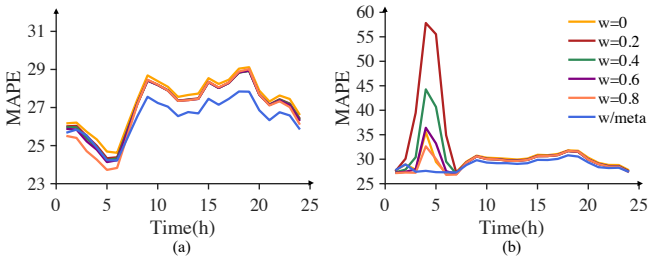

Fig. 15. MAPE performance in various weighing matrices settings: (a) Mobile navigation data, (b) Mobile pedestrian data.

March 28, 2020, into training and testing sets. The module utilized 3,2 and 1 neurons for each MLP layer. We compared the performance of several benchmark models in this section as well:

- Weighted mean approach(WMA) [27] sets the weight according to the error of a single data source to fuse multi sources data.
- Iterative multi-view calibration(IMVC) [41] integrates multi-source data by quantifying biases of data sources and minimizes loss by an iterative learning process.
- Linear regression(LR) [45] adapts the well-known GAN model to minimize the difference between the original and imputed data.
- Gradient Boosting Decision Tree(GBDT) [46] mines the relationship between multi sources data and constructs decision tree to integrate multi sources data.

D. Model Sensitivity Analysis

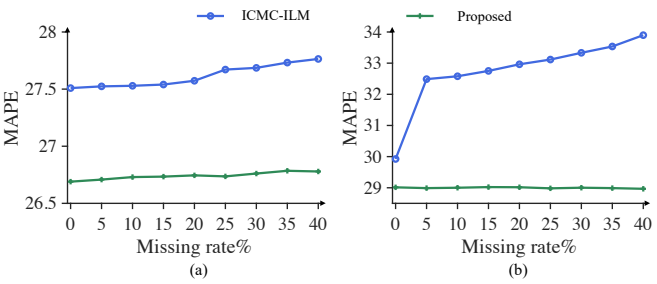

Fig. 16. Comparison of imputation performance under different data missing rate in MAPE: (a) Mobile navigation data, (b) Mobile pedestrian data.

Table IV presents a comprehensive overview of the concrete performance results. It can be concluded that the proposed model outperforms the other models under evaluation. The speed aggregation algorithm effectively mitigates data uncertainty and successfully captures the dependencies present among the multi-source data.

Fig. 13 provides a comparison of the estimation performance across different types of roads in terms of MAPE. It is worth noting that while maintaining high-resolution estimation, the speed estimation accuracy for side roads is slightly lower compared to that of main roads.

In order to validate the effectiveness of the meta-learning process for the weighting matrix, we compare its performance with that of artificially setting the weighting matrix in Fig. 15 (a) and Fig. 15 (b). The results demonstrate that our proposed module effectively learns the intrinsic relationships within the data. It is able to assign higher weights to credible history data, facilitating the imputation process in allocating its attention to different data.

Furthermore, we conducted a comparative analysis of our missing data imputation module against the most competitive model, considering different data missing rates. Fig. 16 depicts the performance of algorithms as the missing rates increase. It shows that even though the performance of algorithms fluctuates as missing rates increase, our proposed model consistently outperforms which demonstrates the robustness and reliability of our algorithm.

E. Ablation Study

To verify effectiveness of different modules and the necessary of introducing multi-source crowdsensing data, we perform ablation studies with four variants::

- **W/O navigation:** W/O navigation is a variant of our proposed model, where the navigation data is removed.
- **W/O pedestrian:** W/O pedestrian is a variant of our proposed model, where the pedestrian data is removed.
- **W/O neighbor:** W/O neighbor is a variant of our proposed model, where the speed aggregation module is removed.
- **W/O external:** W/O external is a variant of our proposed model, where we ignore the external factors.

The outcomes are delineated in Fig. 14. We corroborate the advantages of harnessing multi-source crowdsensing data as opposed to relying on a singular data source. Crucially, our findings demonstrate that the integration of multi-source data does not lead to over-fitting issues but rather enhances

the reliability of the information obtained. We subjected the single data source to the entire model in separate instances and observed a precipitous decline in output performance. The results affirm the evident advantage of our proposed modules, which effectively capture the spatial correlation between roads and significantly enhance the quality of the data.

VI. Conclusion

In this study, we address the enduring challenges of coarse-grained traffic speed estimation methods traditionally used, by introducing an innovative data-driven approach that leverages multi-source implicit crowdsensing data derived from smartphones. By integrating mobile navigation data with mobile pedestrian data, which is incidentally collected from roadside pedestrians when vehicle WiFi signals are scanned by phones, we achieve high-resolution, large-scale traffic speed estimation without necessitating additional costly deployments. To further refine the gathered data, we employ a meta-learning-based matrix decomposition module to impute missing speed data for road segments.Then a self-view speed aggregation algorithm is proposed to utilize the complete spatial information to correct the imputed values. Additionally, we have devised a speed aggregation module to fuse the multi-source recovered data, effectively mitigating uncertainties. To corroborate the efficacy of our approach, comprehensive experiments were conducted with real-world datasets from the city of Wenzhou. The simulation outcomes demonstrate substantial improvements over extant methodologies, evidencing a 7.48% enhancement in data imputation and a 6.99% advancement in data fusion. Looking to the future, we aim to integrate semantic content from geographic information systems and real-time social media data to further augment the estimation accuracy in subsequent studies.

References

[1] Pu Wang, Zhiren Huang, Jiyu Lai, Zhihao Zheng, Yang Liu, and Tao Lin. Traffic speed estimation based on multi-source gps data and mixture model. *IEEE Transactions on Intelligent Transportation Systems*, 23(8):10708 – 10720, 2021.

[2] Zhili Zhou, Xiaohua Dong, Zhetao Li, Keping Yu, Chun Ding, and Yimin Yang. Spatio-temporal feature encoding for traffic accident detection in vanet environment. *IEEE Transactions on Intelligent Transportation Systems*, pages 1–10, 2022.

[3] Bingyu Xu, Yaowei Wang, Zhaozhi Wang, Huizhu Jia, and Zongqing Lu. Hierarchically and cooperatively learning traffic signal control. In *AAAI Conference on Artificial Intelligence*, volume 35, pages 669–677, 2021.

[4] Di Zang, Jiawei Ling, Zhihua Wei, Keshuang Tang, and Jiujun Cheng. Long-term traffic speed prediction based on multiscale spatio-temporal feature learning network. *IEEE Transactions on Intelligent Transportation Systems*, 20(10):3700–3709, 2018.

[5] Yehong Xu, Dan He, Pingfu Chao, Jiwon Kim, Wen Hua, and Xiaofang Zhou. Route reconstruction using low-quality bluetooth readings. In *Proceedings of the 28th International Conference on Advances in Geographic Information Systems*, pages 179–182, 2020.

[6] Tingting Huang. Traffic speed estimation from surveillance video data. In *Proceedings of the IEEE Conference on Computer Vision and Pattern Recognition Workshops*, pages 161–165, 2018.

[7] Xiaomin Fang, Jizhou Huang, Fan Wang, Lihang Liu, Yibo Sun, and Haifeng Wang. Ssml: self-supervised meta-learner for en route travel time estimation at baidu maps. In *27th ACM SIGKDD Conference on Knowledge Discovery & Data Mining*, pages 2840–2848, 2021.

[8] Bo Hui, Da Yan, Haiquan Chen, and Wei-Shinn Ku. Trajnet: A trajectory-based deep learning model for traffic prediction. In *27th ACM SIGKDD Conference on Knowledge Discovery & Data Mining*, pages 716–724, 2021.

[9] Jingru Yu, Marc EJ Stettler, Panagiotis Angeloudis, Simon Hu, and Xiqun Michael Chen. Urban network-wide traffic speed estimation with massive ride-sourcing gps traces. *Transportation Research Part C: Emerging Technologies*, 112:136–152, 2020.

[10] Xinwu Qian and Satish V Ukkusuri. Spatial variation of the urban taxi ridership using gps data. *Applied geography*, 59:31–42, 2015.

[11] Ji Li Zhipeng Cai, Mingyuan Yan, and Yingshu Li. Using crowdsourced data in location-based social networks to explore influence maximization. In *IEEE INFOCOM 2016-The 35th Annual IEEE International Conference on Computer Communications*, pages 1–9. IEEE, 2016.

[12] Fanglan Chen, Zhiqian Chen, Subhodip Biswas, Shuo Lei, Naren Ramakrishnan, and Chang-Tien Lu. Graph convolutional networks with kalman filtering for traffic prediction. In *Proceedings of the 28th International Conference on Advances in Geographic Information Systems*, pages 135–138, 2020.

[13] BH Shekar and Guesh Dagnew. Grid search-based hyperparameter tuning and classification of microarray cancer data. In *2019 second international conference on advanced computational and communication paradigms (ICACCP)*, pages 1–8, 2019.

[14] Jie Cao, Da Wang, Zhaoyang Qu, Hongyu Sun, Bin Li, and Chin-Ling Chen. An improved network traffic classification model based on a support vector machine. *Symmetry*, 12(2):301, 2020.

[15] Weiwei Jiang and Jiayun Luo. Big data for traffic estimation and prediction: a survey of data and tools. *Applied System Innovation*, 5(1):23, 2022.

[16] Zhipeng Cai, Zhuojun Duan, and Wei Li. Exploiting multi-dimensional task diversity in distributed auctions for mobile crowdsensing. *IEEE Transactions on Mobile Computing*, 20(8):2576–2591, 2020.

[17] Benjamin Coifman and SeoungBum Kim. Speed estimation and length based vehicle classification from freeway single-loop detectors. *Transportation research part C: emerging technologies*, 17(4):349–364, 2009.

[18] Amine Haoui, Robert Kavaler, and Pravin Varaiya. Wireless magnetic sensors for traffic surveillance. *Transportation Research Part C: Emerging Technologies*, 16(3):294–306, 2008.

[19] Cheng-Hsun Yang and Hsin-Mu Tsai. Vehicle counting and speed estimation with rfid backscatter signal. In *2019 IEEE Vehicular Networking Conference (VNC)*, pages 1–8. IEEE, 2019.

[20] Jielun Liu, Ghim Ping Ong, and Xiqun Chen. Graphsage-based traffic speed forecasting for segment network with sparse data. *IEEE Transactions on Intelligent Transportation Systems*, 2020.

[21] Zihan Kan, Mei-Po Kwan, Dong Liu, Luliang Tang, Yang Chen, and Mengyuan Fang. Assessing individual activity-related exposures to traffic congestion using gps trajectory data. *Journal of transport geography*, 98:103240, 2022.

[22] Yidan Sun, Guiyuan Jiang, Siew-Kei Lam, Shicheng Chen, and Peilan He. Bus travel speed prediction using attention network of heterogeneous correlation features. In *Proceedings of the 2019 SIAM International Conference on Data Mining*, pages 73–81. SIAM, 2019.

[23] Zhuojun Duan, Wei Li, Xu Zheng, and Zhipeng Cai. Mutual-preference driven truthful auction mechanism in mobile crowdsensing. In *2019 IEEE 39th International Conference on Distributed Computing Systems (ICDCS)*, pages 1233–1242. IEEE, 2019.

[24] Zhuojun Duan, Wei Li, and Zhipeng Cai. Distributed auctions for task assignment and scheduling in mobile crowdsensing systems. In *2017 IEEE 37th International Conference on Distributed Computing Systems (ICDCS)*, pages 635–644. IEEE, 2017.

[25] Honghui Dong, Jie Man, Limin Jia, Xuzhao Wang, Yong Qin, and Kai Liu. Traffic speed estimation using mobile phone location data based on longest common subsequence. In *2018 21st International Conference on Intelligent Transportation Systems (ITSC)*, pages 2819–2824. IEEE, 2018.

[26] Jingqin Gao, Kaan Ozbay, Abdullah Kurkcu, et al. Multi-source data fusion for urban traffic state estimation: A case study of new york city. 2018.

[27] Lin Zhu, Fangce Guo, John W Polak, and Rajesh Krishnan. Urban link travel time estimation using traffic states-based data fusion. *IET Intelligent Transport Systems*, 12(7):651–663, 2018.

[28] Shafiza Ariffin Kashinath, Salama A Mostafa, Aida Mustapha, Hairulnizam Mahdin, David Lim, Moamin A Mahmoud, Mazin Abed Mohammed, Bander Ali Saleh Al-Rimy, Mohd Farhan Md Fudzee, and Tan Jhon Yang. Review of data fusion methods for real-time and multi-sensor traffic flow analysis. *IEEE Access*, 2021.

[29] Lu Lin, Jianxin Li, Feng Chen, Jieping Ye, and Jinpeng Huai. Road traffic speed prediction: a probabilistic model fusing multi-source data. *IEEE Transactions on Knowledge and Data Engineering*, 30(7):1310–1323, 2017.

[30] Li Kuang, Chunbo Hua, Jiagui Wu, Yuyu Yin, and Honghao Gao. Traffic volume prediction based on multi-sources gps trajectory data by temporal convolutional network. *Mobile Networks and Applications*, 25(4):1405–1417, 2020.

[31] Hao Peng, Hongfei Wang, Bowen Du, Md Zakirul Alam Bhuiyan, Hongyuan Ma, Jianwei Liu, Lihong Wang, Zeyu Yang, Linfeng Du, Senzhang Wang, et al. Spatial temporal incidence dynamic graph neural networks for traffic flow forecasting. *Information Sciences*, 521:277–290, 2020.

[32] Paul Newson and John Krumm. Hidden markov map matching through noise and sparseness. In *17th ACM SIGSPATIAL international conference on advances in geographic information systems*, pages 336–343, 2009.

[33] Qianru Sun, Yaoyao Liu, Tat-Seng Chua, and Bernt Schiele. Meta-transfer learning for few-shot learning. In *Proceedings of the IEEE/CVF Conference on Computer Vision and Pattern Recognition*, pages 403–412, 2019.

[34] Haoxiang Wang, Han Zhao, and Bo Li. Bridging multi-task learning and meta-learning: Towards efficient training and effective adaptation. In *International Conference on Machine Learning*, pages 10991–11002, 2021.

[35] Ondrej Bohdal, Yongxin Yang, and Timothy Hospedales. Evograd: Efficient gradient-based meta-learning and hyperparameter optimization. *Advances in Neural Information Processing Systems*, 34:22234–22246, 2021.

[36] Chelsea Finn, Pieter Abbeel, and Sergey Levine. Model-agnostic meta-learning for fast adaptation of deep networks. In *International conference on machine learning*, pages 1126–1135. PMLR, 2017.

[37] Ondrej Bohdal, Yongxin Yang, and Timothy Hospedales. Evograd: Efficient gradient-based meta-learning and hyperparameter optimization. *Advances in Neural Information Processing Systems*, 34:22234–22246, 2021.

[38] B Vinodh Kumar and Thuthi Mohan. Sigma metrics as a tool for evaluating the performance of internal quality control in a clinical chemistry laboratory. *Journal of laboratory physicians*, 10(02):194–199, 2018.

[39] Wenguang Song, Mykola Beshley, Krzysztof Przystupa, Halyna Beshley, Orest Kochan, Andrii Pryslupskyi, Daniel Pieniak, and Jun Su. A software deep packet inspection system for network traffic analysis and anomaly detection. *Sensors*, 20(6):1637, 2020.

[40] Wenjie Du, David Côté, and Yan Liu. Saits: Self-attention-based imputation for time series. *Expert Systems with Applications*, 219:119619, 2023.

[41] Desheng Zhang, Tian He, and Fan Zhang. National-scale traffic model calibration in real time with multi-source incomplete data. *ACM Transactions on Cyber-Physical Systems*, 3(2):1–26, 2019.

[42] Jinsung Yoon, James Jordon, and Mihaela Schaar. Gain: Missing data imputation using generative adversarial nets. In *International conference on machine learning*, pages 5689–5698. PMLR, 2018.

[43] MN Noor, AS Yahaya, Nor Azam Ramli, and Abdullah Mohd Mustafa Al Bakri. *Filling missing data using interpolation methods: Study on the effect of fitting distribution*, volume 594. Trans Tech Publ, 2014.

[44] Shichao Zhang. Nearest neighbor selection for iteratively knn imputation. *Journal of Systems and Software*, 85(11):2541–2552, 2012.

[45] George AF Seber and Alan J Lee. *Linear regression analysis*. John Wiley & Sons, 2012.

[46] Lan Zhang. Design of a sports culture data fusion system based on a data mining algorithm. *Personal and Ubiquitous Computing*, 24(1):75–86, 2020.